Reinforcing ethyl cellulose aerogels with poly(lactic acid) for enhanced bone regeneration

Gabrijela Horvat · Jan Rožanc · Uroš Maver ·
Matjaž Finšgar · Željko Knez · Zoran Novak

Abstract Developing double porous biodegradable and biocompatible scaffolds that can incorporate and release drugs in a controlled manner holds immense potential in regenerative medicine. This study presents a synthesis method for preparing a macro-mesoporous scaffold, where poly(lactic acid) adds to the macroporous region and mechanical properties, and ethyl cellulose adds to the surface area ($182 \ m^2/g$). High surface area enables the incorporation of model drug indomethacin with an entrapment efficiency of 17.0% and its later controlled release profile. The resulting scaffold has desirable mechanical properties in the range of a natural trabecular bone with a compressive modulus of 22.4 MPa. The material is stable in the simulated body fluids for 120 days before the slow degradation starts. *In vitro* studies demonstrate the material's ability to support bone cell adhesion, proliferation, and differentiation, promoting osteogenic activity. Overall, the unique combination of poly(lactic acid) and ethyl cellulose produces advanced materials with tailored macro and mesopore properties, remarkable mechanical properties, optimal degradation rate, and drug delivery potential, making it a promising candidate for bone scaffolds in regenerative medicine and tissue engineering.

Introduction

The size of the ageing population over 60 will continue to grow in the coming years and is expected to double by 2050 (WHO 2022; Eurostat n.d.)**.** Among the common age-related conditions is osteoarthritis, affecting more than 50% of the population over 65 years. Combining osteoarthritis-related fractures with an increasing number of accidents and trauma cases, the demand for bone implants is expected to grow (Mastnak et al. 2022)**.** Today, most implants are made from metal (medical grade stainless steel titanium alloys), ceramics and bioglasses (Ribas et al. 2019)**.** Such implants are inserted into the body surgically to support the damaged bone or joint. The main disadvantage of these implants is the need for revision surgeries (with an increasing life expectancy, the number of revisions rises) and/or implant-associated infections, which are considerably high (2–5% of all primary implantation surgeries) (Wu et al. 2022)**,** and as such further contribute to implant rejection.

G. Horvat · M. Finšgar · Ž. Knez · Z. Novak (✉)
Faculty of Chemistry and Chemical Engineering, University of Maribor, Smetanova Ul.17, 2000 Maribor, Slovenia
e-mail: zoran.novak@um.si

J. Rožanc · U. Maver · Ž. Knez
Medical Faculty, University of Maribor, Taborska Ul. 8, 2000 Maribor, Slovenia

Prospective bone implants are increasingly viewed as host materials that serve as temporary scaffolds. When integrated into the body, they provide sufficient support, like native bones, while simultaneously promoting bone growth. Such materials often deliver bioactive substances to promote bone regeneration further or aid better clinical outcomes (Nie et al. 2022).

An "ideal" artificial bone implant material should be biocompatible and biodegradable with a controllable degradation rate, whereas the degradation products should be non-toxic (Pradhan et al. 2020). Other crucial characteristics of such implants include a high porosity with an interconnected architecture of pores with a controlled shape, size, and alignment to facilitate oxygen nutrients and waste transfer. Such internal geometries are known to, among others, promote rapid vascularisation and tissue in-growth (Junior Maksoud et al. 2022). They should resist stress, hold good mechanical properties, be clinically compliant, and need to pass *in-vitro* and *in-vivo* biocompatibility tests (Liu et al. 2019).

The pore size is among the most important properties for a bone implant to succeed (Abbasi et al. 2020). It was shown that bone ingrowth improves when the pore size is about 80–200 µm. Such pores allow cell colonization, migration and transport. However, only pores of 300–500 µm enable the formation of capillaries, which should be considered concerning more vascularised tissues (Fernandez de Grado et al. 2018). Another critical parameter in designing effective implants is the antimicrobial capacity. To minimize infections, a local controlled drug release is desired (Weiser and Saltzman 2014). Furthermore, contact microbe growth inhibition (e.g., in situ antimicrobial activity) provides a good foundation to prevent biofilm formation even after implant infection (Peeters et al. 2019).

In past years, processing with supercritical fluids, mainly supercritical CO_2, has been evaluated extensively (Kravanja et al. 2022). Supercritical technology allows the processing of polymers and inorganic materials at mild operating conditions, resulting in final materials that are completely free of organic solvents (Knez et al. 2014). Additionally, it enables the design of materials of different compositions (organic, inorganic, or hybrid), morphology (micro- and nanoparticles, monoliths, beads, sponges), porosity (meso- and macro-porosity), and inner architecture (homogeneous, multi-component, multi-layered). Moreover, processing with supercritical and near-critical fluids produces a solvent-free end-product with high purity. Among the most interesting materials prepared by supercritical technology are aerogels (García-González and Smirnova 2013).

Aerogels are a class of advanced solvent-free materials that can be easily prepared from biodegradable and biocompatible resources. Their extremely high surface areas promote cell adhesion and proliferation, as well as the incorporation of other agents like pharmaceuticals (antibiotics, anti-inflammatory agents, etc.) (García-González et al. 2021). The properties of aerogels are tuneable (morphology, pore size distribution, composition, density) through the sol–gel process by which they are prepared (Dervin and Pillai 2017). The processing parameters during the sol–gel method and the supercritical drying process (Kistler 1931) are chosen based on the desired properties of the material. For example, the sol–gel process allows the formulation of final materials with a specifically determined drug release profile (e.g., immediate, controlled, and delayed release) (Horvat et al. 2018). In addition, their structure can mimic the properties of various tissues (e.g., bone), whereas their interconnected pores provide an excellent structure for cell growth. Biodegradable aerogels are prepared mainly from polysaccharides, such as pectin(Veronovski et al. 2014), alginate(Horvat et al. 2016), and cellulose(Pircher et al. 2016).

Ethyl cellulose (EC) is one of the cellulose derivatives, where the ethoxy groups have replaced the hydroxyl groups on the repeating glucose units. EC is considered safe and is included in the U.S. Food and Drug Administration (FDA) Inactive Ingredients Database. It is a non-ionic material and non-reactive in the body (Wasilewska and Winnicka 2019). EC is biocompatible and non-allergenic, does not dissolve in water, and is stable in body fluids for longer periods. EC is chemically stable and less prone to hydrolysis compared to other cellulose derivatives such as methyl cellulose or hydroxypropyl cellulose. This stability is beneficial for long-term applications, such as medical devices. Like most polysaccharides, it can form gels (Davidovich-Pinhas et al. 2015). The latter enables EC to control drug release (Choy et al. 2009; Wang et al. 2023) or to form a pH dependent

drug release (Tran et al. 2021). Compared to other cellulose derivatives, such as hydroxypropyl cellulose, hydroxyethyl cellulose, carboxymethyl cellulose and methyl cellulose, EC is hydrophobic. Hydrophilicity of other derivatives can be a disadvantage because it can cause the scaffold to swell or degrade over time, leading to a loss of mechanical integrity and therefore in this sense, EC is a better choice for bone implant scaffolds.

The mechanical properties of polysaccharide aerogels are, regretfully, not in the range of bone implants (Muhammad et al. 2021). Therefore, adding a secondary material is highly desired for providing better mechanical stability and hence better mimicking the properties of the native bone (Oladapo et al. 2020). Such material should also be biocompatible, biodegradable, and not hinder the base aerogel microporous structure. Polylactic acid (PLA) has gained great attention due to its natural degradability, biocompatibility, and processibility. The PLA is hydrolyzed naturally into lactic acid and converted into water and carbon dioxide in the human body. It can provide good mechanical properties in the range of a trabecular bone and, with some modifications, even that of cortical bone (Zan et al. 2022). One of the limitations of PLA as bone graft materials is its limited osteogenic activity, which may be improved by the addition of inorganic (Melo et al. 2019) or organic (Mao et al. 2018; Janmohammadi et al. 2022) fillers. Ethyl cellulose is one of the polysaccharides that is known for its biocompatibility and good osteogenic properties (Tian et al. 2014). Such composite material can incorporate drugs for local treatment in order to alleviate pain or reduce inflammation in bone implants. Indomethacin (IND) is a nonsteroidal anti-inflammatory drug (NSAID) that can be used to treat such conditions and was therefore chosen as a model drug in this research. This drug is poorly water soluble. In supercritical carbon dioxide the solubility at 272 bar is 2.96×10^{-5} (Kloc et al. 2023), which is considered poorly soluble and may be suitable for the incorporation into aerogels and supercritical CO_2 processing. Thus, developing macro-mesoporous PLA-EC aerogels by using supercritical CO_2 (green chemistry) with good mechanical properties, and drug delivery potential results in promising materials for regenerative medicine.

Materials and methods

Materials

EC (48.0–49.5% w/w ethoxyl basis, viscosity range 30–70 cP, CAS: 9004–57-3; CAT: 46080; Sigma Aldrich, Missouri, USA), PLA (Goodfellow, granular, molecular weight: 230 kg/mol, 3 mm nominal granule size, CAT: GF45989881; Sigma Aldrich, Huntingdon, U.K.), chloroform (ACS reagent, ≥ 99.8%, Sigma Aldrich, Munich, Germany), ethanol (ACS reagent, ≥ 99.5%, Sigma Aldrich, Munich, Germany), indomethacin (IND) (analytical grade, ≥ 99% purity, Sigma Aldrich, Missouri, USA). Osteoblast Growth Medium Supplement Mix (PromoCell, Heidelberg Germany), penicillin (PromoCell, Heidelberg Germany), streptomycin (PromoCell, Heidelberg Germany), fixative solution (Merck KGaA, Darmstadt, Germany), phalloidin conjugate (Abcam, U.K.), bovine serum albumin (BSA; Sigma-Aldrich, Munich, Germany), Tween 20 (Sigma-Aldrich, Munich, Germany), Alamar Blue (Santa Cruz, Dallas, TX, USA), protein markers: Rb pAb anti-COLIA1, Rb pAb anti-OCN, and Goat pAb to Rb- AF 594 (all Abcam, Cambridge, UK). All other reagents used were of analytical grade.

Fabrication of scaffolds

Sol–gel templating of EC-PLA scaffolds

For EC-PLA scaffold formation (Scheme 1), a 4 wt% solution of EC in ethanol was prepared at 70 °C in a sealed beaker and then cooled to room temperature. The 4 wt% PLA solution was prepared in chloroform at room temperature in a sealed beaker to prevent evaporation. Then, the homogeneous PLA solution was poured into the previously prepared EC solution under constant stirring at 600 rpm to enhance uniformity. Once all the PLA solution was added, the stirring continued for another 1 min, after which the solution was transferred to a mold to form a gel. The resulting monolith was stored in ethanol for 16 h before supercritical drying.

Preparation of the reference materials

The reference EC and PLA scaffolds were prepared to evaluate and characterize the EC-PLA scaffolds.
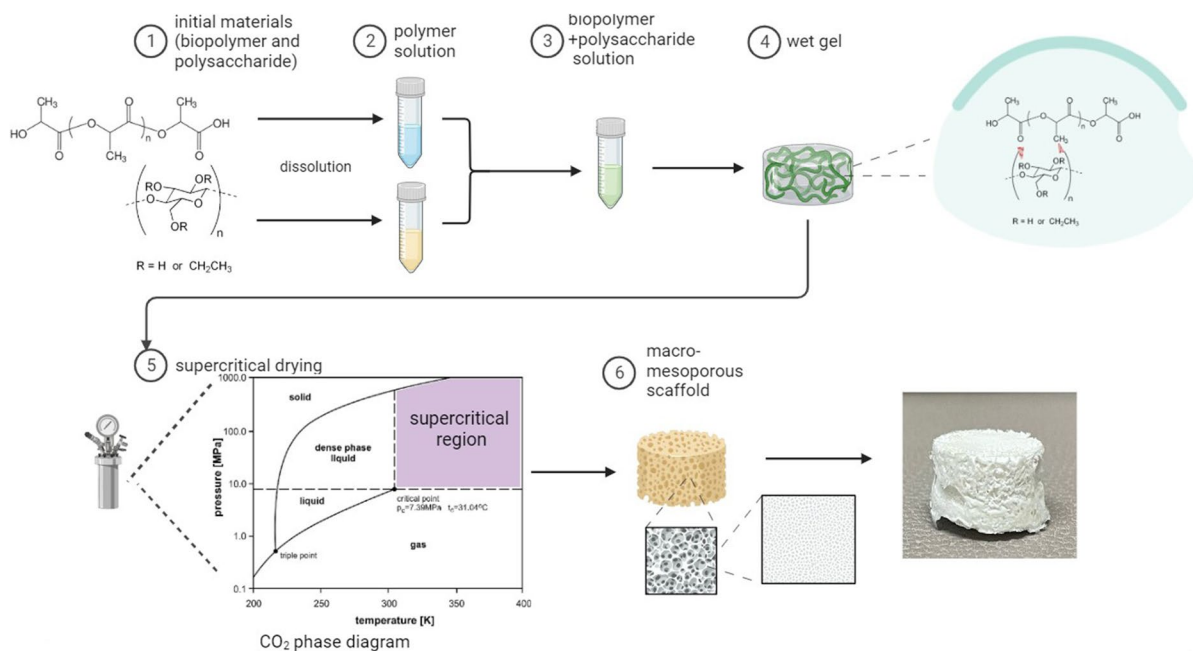
Scheme 1 Schematic illustration of the synthesis process for the EC-PLA scaffolds

The 4 wt% EC solution in ethanol was prepared at 70 °C in a sealed beaker. The solution was cooled to room temperature, and ultrapure water was added to the solution (1:1 w/w), forming a soft cylindrical-shaped gel. The PLA scaffold was prepared by dissolving 4 wt% of PLA in chloroform, and then this solution was poured into ethanol (1:1 w/w) while stirring, obtaining a soft gel. Both reference materials were then dried supercritically.

Preparation of EC-PLA-IND scaffolds

The EC-PLA-IND sample was prepared by the same sol–gel templating as the EC-PLA scaffold but with the addition of IND. Due to its good ethanol solubility, the drug was incorporated in the gel preparation step by adding it to the EC solution. The EC solution in ethanol (4 wt%) was prepared at 70 °C, cooled, and IND (0.4 wt%, which corresponds to 100 mg) was added during stirring at 600 rpm. The PLA solution was then added. Sol–gel templating of EC-PLA scaffolds. The sample EC-PLA-IND was stored in an indomethacin-saturated ethanol solution before supercritical drying.

Supercritical CO$_2$ drying

Supercritical drying of the prepared samples was performed on the modified supercritical extraction unit (UHDE GmbH., Dortmund, Germany). The scaffolds were placed into a 500 mL autoclave, preheated to 42 °C and filled with ethanol. Then the system was pressurized up to 120 bar, and the ethanol extraction from samples was performed for 6 h at a CO$_2$ flow rate of approximately 200 L h^{-1}. The system was then depressurized slowly and left to cool down to room temperature. Finally, the dried scaffolds were taken from the autoclave and stored in a desiccator (Kistler 1931; Novak and Knez 1997).

Scaffold characterization

Physical properties and mechanical analysis

Micrographs of the prepared scaffolds were obtained using a field emission scanning electron microscope (FE-SEM) Sirion 400 NC (FEI, Eindhoven, The Netherlands) operated with an accelerating voltage of 10 kV and using a W.D. detector. The scaffolds were sputter-coated with gold particles and fixed to

aluminium sample holders with double-sided carbon tape and scanned at 2000x (20 μm scale bar) and 64000x (1 μm scale bar).

Shrinkage of the material was observed by measuring the size of the wet and dry sample (length, width, height) with electronic calliper. Three samples were measured, and the shrinkage was calculated as the volume shrinkage by the Eq. (1):

$$\eta = 1 - \frac{V_{dry}}{V_{wet}} \qquad (1)$$

where η us the volume shrinkage, V_{dry} is the volume of the dry scaffold and V_{wet} is the volume of the prepared wet scaffold.

Apparent density of EC-PLA scaffold was determined by density analyzer GeoPyc 1365 Micromeritics. The surface area (BET) was determined by the nitrogen adsorption measurement (Micromeritics ASAP 2020, Norcross, GA, USA). The sample was degassed for 10 h at 70 °C and then analysed with nitrogen at -196 °C.

The thermal transitions were studied by a differential scanning calorimeter (DSC) and thermal gravimetry (TGA) within an N_2 atmosphere (50 mL/min) with a 10 °C/min heating rate. The analysis was performed on an HP DSC1 Mettler Toledo apparatus (TGA/DSC1, Mettler Toledo AG (MTANA), Zürich, Switzerland). The temperature range of the analysis was set at 20–600 °C.

ATR-FTIR spectra of the PLA, EC-PLA, and EC were measured using a IRAffinity-1 FTIR spectrometer (Shimadzu, Kyoto, Japan), with an attenuated total reflection (ATR) module at a scan range of 4000–600 cm^{-1}. The FT-NIR spectra were recorded on a Fourier-transform near infrared spectrometer (Matrix-F, Bruker Optics, Ettlingen, Germany) from 12,000 to 4000 cm^{-1} in absorbance mode. For each sample, 64 scans were obtained with a spectral resolution of 4 cm^{-1} and then averaged. The presented spectra are an average of 32 consecutive measurements.

ToF–SIMS measurements were performed using an M6 device (IONTOF, Münster, Germany) equipped with a Bi liquid metal ion gun. The primary beam was 30 keV Bi_3^+ at a target current of 0.6 pA. The charge neutralizer was on during the measurement, and a surface potential was applied in both polarities. To obtain 3D profiles, the surface was sputtered with a gas cluster ion beam (GCIB) using Ar_{1900}^+ clusters at an acceleration voltage of 2.5 keV and a target current of 50 pA. Sputtering was performed on an area of 500 by 500 μm, and an analysis was made in the centre of the sputter crater at 300 by 300 μm. The spectra were calibrated using known peaks at certain mass-to-charge ratios (m/z), i.e. C^- at m/z 12.00, C_2^- at m/z 24.00, C_3^- at m/z 36.00, and C_4^- at m/z 48.00 in negative polarity, and $C_2H_3^+$ at m/z 27.02. $C_3H_5^+$ at m/z 41.04, $C_4H_5^+$ at m/z 53.04, and $C_4H_7^+$ at m/z 55.05 in positive polarity.

The mechanical analysis was performed on a universal testing machine (Shimadzu AG–X plus 10 kN). The samples were prepared in a cylindrical shape with a height of ~10 mm and a diameter of ~20 mm. The compression strain was estimated as h/h_0, where h is the deformed height, and h_0 is the original height. The compression stress was measured as F/A_0, where F is the force applied on the scaffold and A_0 is the actual cross-section area of the sample. The compression rate was 50 mm/min. The samples' tensile strength and elongation percentage at break (Eb) were determined, together with the E-modulus.

Swelling and stability

The structural stability and integrity in simulated body fluid (SBF) were evaluated for 13 weeks at 37 °C. The EC-PLA-IND samples were immersed into the SBF, prepared as described previously in (Kokubo et al. 1990) with ion concentrations of 142.0 mM Na^+, 5.0 mM K^+, 1.5 mM Mg^{2+}, 2.5 mM Ca^{2+}, 148.8 mM Cl^-, 4.2 mM HCO_3^-, 1.0 mM HPO_4^{2-}, and 0.5 mM SO_4^{2-}. The pH of the SBF was adjusted at pH 7.40 at 36.5 °C with 1 M HCl. The wet weight was measured after 15 min equilibration and at different intervals from 1 to 213 days of immersion. The weight variation was calculated using Eq. (2):

$$weight\ variation\,[\%] = (1 - \frac{w_{tn}}{w_{15min}}) \cdot 100, \qquad (2)$$

where w_{tn} and w_{15min} stand for the wet weights of the samples at the certain time and after 15 min of swelling, respectively.

Indomethacin drug content and *in vitro* release

Indomethacin content

The sample was poured into 10 mL of ethanol (in a sealed beaker) for 96 h under constant stirring

conditions at 500 rpm. After 96 h, the drug amount was determined spectrophotometrically using Cary 50 Probe UV spectrophotometer (Agilent Technologies, Santa Clara, California) at a wavelength of 245 nm. The mass of the drug (m_d) was determined based on the calibration curve methodology. The drug content (D.C.) was calculated from Eq. (3):

$$D.C.[\%] = \frac{m_d}{m_s} \cdot 100, \tag{3}$$

where m_d is the mass of the drug (mg), and m_s is the initial mass of the weighted aerogel sample. Each test was made in triplicate, and the average values were calculated along with standard deviations.

In-vitro drug release of indomethacin

For the *in vitro* drug release testing, phosphate-buffered saline (PBS) with pH 6.8 was prepared by mixing 250.0 mL of 0.2 M KH_2PO_4 and 112.0 mL 0.2 M NaOH and diluting to 1000.0 mL with ultrapure water. Drug dissolution tests of the EC-PLA-IND were performed in PBS with pH 6.8. The analysis was performed for 50 days. After 45 days the 100% release was achieved. The drug dissolution studies were performed in triplicate at 37 ± 0.5 °C, employing the USP I apparatus (708-DS, Agilent Technologies). The rotation speed was set at 50 rpm, and the volume of the dissolution media was 900 mL, according to E.U. Pharmacopoeia. Aliquots (2 mL) were withdrawn at the certain time periods and analysed spectrophotometrically at a wavelength of 267 nm. Sampling was performed after 1 h, 2 h, 5 h, 7 h, 12 h, 18 h, 24 h, and each day up to 3 weeks. Later, the sampling was performed after 6 and 7 weeks. The cumulative release was calculated by Eq. (4).

$$cumulative\ release\ [\%] = \frac{c \cdot V}{m_t} \cdot 100, \tag{4}$$

where c is the concentration of the IND in the release medium after the selected time intervals in mg/mL, V is the volume of the release medium in mL, and m_t is the total amount of the drug within the release medium in mg, obtained after 7 weeks of the dissolution test. The drug dissolution test was performed in triplicate.

Biocompatibility analysis

The biocompatibility analysis was performed using primary human osteoblasts (HOB) isolated from trabecular femoral tissue. The cells were cultured in an osteoblast growth medium supplemented with Osteoblast Growth Medium SupplementMix and 1% penicillin/streptomycin. Before testing, all the samples were sterilized under UV light for 30 min and placed in 24-well plates.

Cell viability

To assess cell viability, the cells were placed directly on the scaffolds. The cells were incubated on the scaffolds for 24 h and 72 h, respectively. After incubation, the viability of live and dead cells was determined using Calcein-AM/P.I. (Sigma-Aldrich, Germany), and the samples were imaged using a fluorescence microscope EVOS FL (Thermo Fisher Scientific, Manassas, VA, USA).

Cell morphology

To assess cell morphology, the cells were fixed after 48 h with a fixative solution and stained with red fluorescent phalloidin conjugate, 1/1000 dilution, in PBS containing 1 wt% bovine serum albumin and 0.1 wt.% Tween 20 to visualize the actin filaments. A Fluoroshield mounting medium containing 4',6-diamidino-2-phenylindole DAPI was used as a counterstain to visualize the cell nuclei.

Cell metabolic activity

The Alamar Blue (Resazurin) assay was performed to determine the cells' metabolic activity. The cells were seeded at a density of 4×10^4 cells per well in a 24-well plate on the scaffolds. Cells seeded on tissue culture (TC) plates were used as positive controls. On days 1, 3, and 7 the cells were treated with 10 µg/mL Alamar Blue and incubated at 37 °C for 4 h. The fluorescence intensity of each sample was measured at an excitation wavelength of 530/25 nm and an emission wavelength of 590/35 nm using the Varioskan Flash multiwell plate reader (Thermo Scientific, Manassas, VA, USA). The cell medium was changed on day 3.

Phenotypic analysis

The protein expression of collagen type I (COLIA1) and osteocalcin (OCN) was examined to determine the phenotypic markers of the exposed cells. Briefly, the cells were seeded at a concentration of 2.5×10^4 cells/well onto samples placed in a 24-well plate and incubated for 10 days. The medium was changed twice a week. After incubation, the cells were fixed with a fixative solution. The following antibodies were used for immunostaining to assess the expression of protein markers: Rb pAb anti-COLIA1, Rb pAb anti-OCN, and Goat pAb to Rb- AF 594.

Statistical analysis

All data were collected from at least three parallel tests and the results are reported as the mean ± standard deviation. Statistical analyses were performed using SPSS 23.0 software. Analysis of variance (ANOVA) was employed to determine significant differences between groups, and the statistical significance was set at $p < 0.05$.

Results and discussion

Formation of the EC-PLA and EC-PLA-IND scaffolds

The formation of EC-PLA scaffolds in which PLA provides mechanical stability and adds to the macroporosity of the material and EC adds the mesoporosity, drug loading, and faster degradability, requires initial optimization of the processing parameters. Since EC is not soluble in water like most other polysaccharides, different solvents were tested to dissolve it before further use, i.e. ethyl lactate, ethanol, N-methyl-2-pyrrolidone, and vegetable oil. Ethanol was selected as the final solvent in this process due to the its propensity for the gelation upon contact with PLA in chloroform, while the concentration was set to 4 wt%, based on the solution's viscosity and our previous research on polysaccharide solutions for aerogel preparations (Tkalec et al. 2015). Similarly, the PLA was dissolved in different solvents (chloroform, ethyl lactate, acetonitrile, dichloromethane) in order to check the suitable solvent for the gel formation with EC solution. The final solution was prepared in chloroform (4 wt%), as it was observed that combining the EC solution in the ethanol and PLA solution in chloroform can result in gel formation upon contact. All other combinations of solvents did not result in a gel formation. Since EC is also soluble in chloroform, the single solvent system could potentially be used for the preparation of the scaffolds. However, no gelation occurred from this combination of solvents and polymers. Further on, after choosing the solvents for both polymers, the ratio between both solutions had to be determined based on the capability to form the desired macro-mesoporous structure of the final material. After aiming different combinations (EC:PLA (w/w) = 1:1, 2:1, 5:1 10:1), the 1:1 w/w EC:PLA was chosen as the most suitable for the final application due to the higher surface area and mechanical stability. Higher ratios of PLA were not used, since good mechanical properties were achieved in this combination since the purpose was to provide a higher surface area for the incorporation of drugs. The gelation mechanism between EC and PLA involves different interactions. Both EC and PLA have functional groups that can participate in hydrogen bonding, i.e. hydroxyl groups of EC and carbonyl group of PLA. Such hydrogen bonds promote polymer chain interaction and contribute to gel formation. Additionally, due to their similar hydrophobic nature, both polymers exhibit some degree of compatibility, which enables the formation of a network structure. Supercritical drying was chosen as the most suitable drying method to preserve the structure of the wet material. Supercritical drying is a method that enables the removal of the liquid from the material without causing structural collapse or shrinkage. The material is placed in a chamber in which the pressure and temperature are elevated to reach the supercritical state of CO_2. At such conditions, the CO_2 can extract the solvent (i.e. ethanol) without undergoing a liquid-to-gas phase change, thus preventing the collapse or distortion of the gel structure. This process allows the solvent to be removed while minimizing the capillary forces that would otherwise cause the collapse or shrinkage of the gel's network.

IND was chosen as a model drug in this research for its non-steroidal anti-inflammatory properties, which can also benefit the targeted application as part of bone implants (Mccarthy et al. 1991). Furthermore, various articles report its potential influence on the growth of osteoblasts, although some

reports also describe its negative effects on new bone formation (Chow and Chambers 1994; Kapur et al. 2003). Despite these contradictory findings, we have shown in our previous studies that NSAIDs can improve bone cell growth (Finšgar et al. 2016, 2021; Maver et al. 2018), which was found also for IND (Horvat et al. 2017). This drug has limited solubility in water as it belongs to BCS Class II (highly permeable with low solubility) (FDA 2016). However, its solubility in ethanol is much higher than in water, and it can reach up to 50 mg/mL upon stirring. The IND was therefore added to the EC-ethanol solution (0.4 wt%). The final drug loading was 18.8 mg/g, and the entrapment efficiency was 17.0%, accounting that the 100 mg of the drug was used for one sample. The entrapment efficiency is governed by the loss of indomethacin during the addition of ethanol prior the supercritical drying since indomethacin is soluble in alcohol. The loss during the supercritical drying is neglectable due to the poor solubility of IND in supercritical carbon dioxide (Kloc et al. 2023). To improve the entrapment efficiency, the drying without additional ethanol in autoclave could be performed, but

it could also affect the structure of the final material because of evaporation drying. Both scaffolds, EC-PLA and EC-PLA-IND, showed no shrinkage during the supercritical drying step. This effect is highly important in the preparation of aerogels. The apparent density of EC-PLA was determined to be 0.4425 ± 0.0019 g/cm^3 and the surface area 182 ± 22 m^2/g (isotherm shown in the Fig. 1b). The surface area of PLA was 31 m^2/g, while EC exhibited a larger surface area of 194 m^2/g m^2/g. However the surface area of EC-PLA-IND was significantly lower at 2.4 m^2/g, likely because of the pore blockage caused by indomethacin. Pore volumes and pore sizes were determined from the desorption side of the branch, however it has to be mentioned, that the numbers obtained are only representative for the mesoporous part of the samples, since the nitrogen adsorption is only valid in this range (Horvat et al. 2022). Pore volumes of EC-PLA, EC-PLA-IND, PLA and EC were 0.73, 0.004, 0.076 and 0.66 cm^3/g, respectively. Average mesopore size of prepared samples was 13.8, 28.9, 9.8 and 14.5 nm for EC-PLA, EC-PLA-IND, PLA and EC, respectively. This data shows the low available volume in
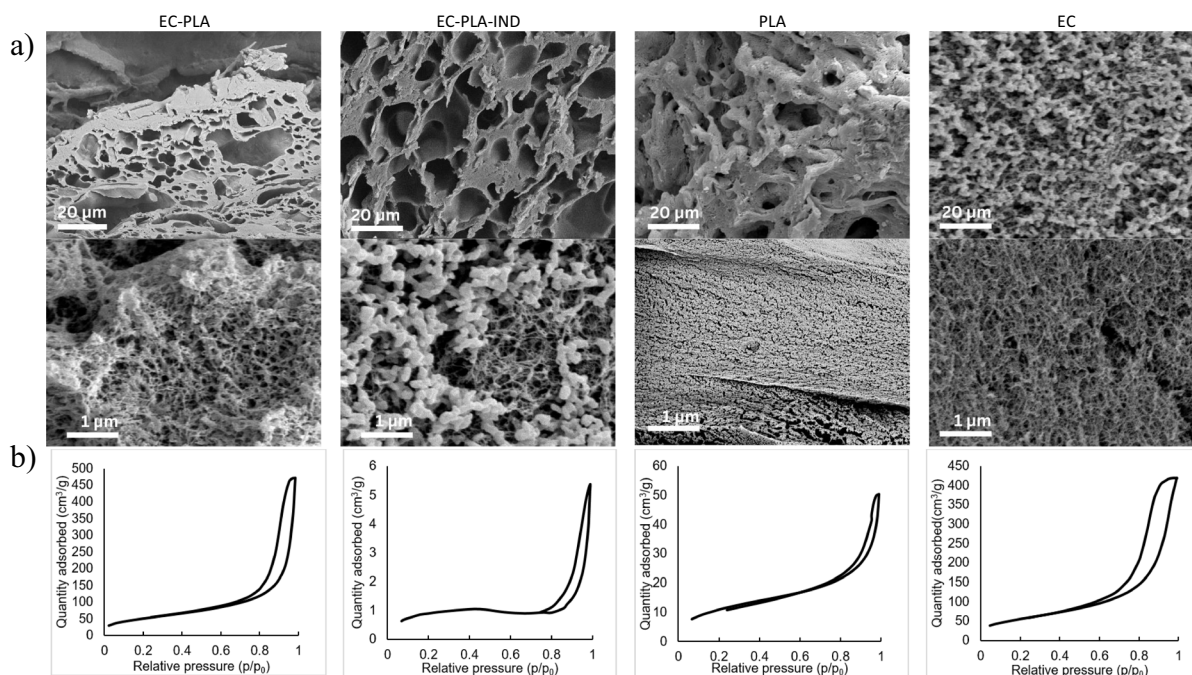

Fig. 1 Sample characterization. **a** Scanning Electron Micrographs at low (above) and high magnification (under) and **b**) nitrogen adsorption isotherms of the EC-PLA scaffold, the EC-PLA-IND scaffold, the PLA scaffold, and EC scaffold

drug-loaded samples and higher average pore size, which is probably due to the dominant presence of indomethacin filling the majority of the pores. The EC sample presents typical mesoporous sample while pure PLA sample has lower surface area and available mesoporous volume as also seen on the SEM micrographs. The SEM micrographs, showing sample morphologies of both samples, are presented in Fig. 1. The latter also includes the PLA sample for comparison. The micrographs show that the EC-PLA scaffold has a highly interconnected, open-pore porous structure with larger macropores, as also found for the PLA sample (Fig. 1a). Oppositely, the EC aerogel typically has a mesoporous structure, with pores ranging from 2–50 nm as reported in our previous publication (Rege et al. 2016; Horvat et al. 2022). The lack of macropores in bioaerogels and their friability is the main reason for their limited applicability in tissue engineering (Ferreira-Gonçalves et al. 2021). As described above, both scaffold materials were prepared by mixing two solutions, excluding chemical reactions between the two components. The PLA, in this case, adds to the desired macroporosity, which is crucial for cell growth (Fig. 1a). The macroporous structure of PLA is already reported in the literature (Chen et al. 2022). The porous structure seems interconnected (Fig. 1a), which is essential for tissue engineering applications since such internal geometries promote cell colonization and enable migration into the scaffold interior (Lutzweiler et al. 2020). The walls between the macropores are highly porous, with pores in the range of mesopores (observed from the magnified picture of the EC-PLA sample). The mesoporous structure of the EC-PLA is uniform (Fig. 1a). This characteristic is highly favourable for incorporating pharmaceuticals, such as IND. The incorporation of IND influenced the internal structure's uniformity and lowered the available mesopores (Fig. 1b). The latter might be partially explained through the added IND, which was filling the mesopores. The EC structure is highly mesoporous with the mesopores in the range as expected based on the literature report on cellulose aerogels (Coquard and Baillis 2017; Rege et al. 2018).

The molecular structure of the samples was characterized by FTIR spectroscopy (Fig. 2a). The latter method was used to detect potential chemical

reactions between the EC and PLA in the composite scaffold. In addition, the IR spectra were measured to confirm the presence of both components (EC and PLA) in the final material. The PLA shows characteristic stretching of C=O and C-O at 1755 and 1089 cm^{-1}, respectively. Bending for -CH_3 asymmetric and -CH_3 symmetric have been identified at 1454 and 1367 cm^{-1}, respectively. The EC aerogel showed bands at 3637, 3498, and 3728 cm^{-1}, characteristic for -OH stretching vibrations. The stretching of -CH_2- and -CH_3 is visible at 2862 cm^{-1}. The IR spectra of the EC-PLA scaffold showed the same characteristic bands as the reference PLA and EC aerogels, showing that the scaffold was composed of both polymers. The latter was further confirmed since no additional band was generated in the spectra of the EC-PLA scaffold, showing that both polymers were interconnected and that no chemical reaction between them was involved. Strong band at 2349 cm^{-1} is attributed to O=C=O stretching of carbon dioxide.

The FT-NIR spectra were measured (Fig. 2b) to confirm the presence of IND in the EC-PLA-IND sample. The IND (powder) spectra were compared to the EC-PLA and EC-PLA-IND scaffolds. Characteristic bands for IND were detected in the EC-PLA-IND spectra at 4088 cm^{-1} and 5900 cm^{-1}, confirming the presence of the IND in the sample. Moreover, characteristic bands for EC-PLA were present in the EC-PLA-IND sample at 8530 cm^{-1}, 5250 and 5200 cm^{-1}.

Thermal stability and mechanical properties

The thermal properties of the EC-PLA scaffolds were investigated using TGA and DSC. The DSC thermograms of the reference samples and the EC-PLA scaffold are presented in Fig. 3a. The TGA curve of the reference EC aerogel agrees with the previous report for the EC polymer (Mao et al. 2018). Therefore, preparing the aerogel sample does not affect the thermal properties of this raw material. A similar is true for the PLA, where the thermogram of the reference PLA aerogel matches well with that for the pure PLA polymer reported previously (Cuiffo et al. 2017). However, the thermogram of the composite EC-PLA scaffold prepared in this research shows the characteristics of EC and PLA, as expected. The first melting point of PLA is matching with the one from

Fig. 2 a ATR-FTIR spectra of the reference materials (PLA and EC) and EC-PLA scaffold. **b** FT-NIR spectra of the indomethacin (IND), EC-PLA, and EC-PLA-IND scaffolds
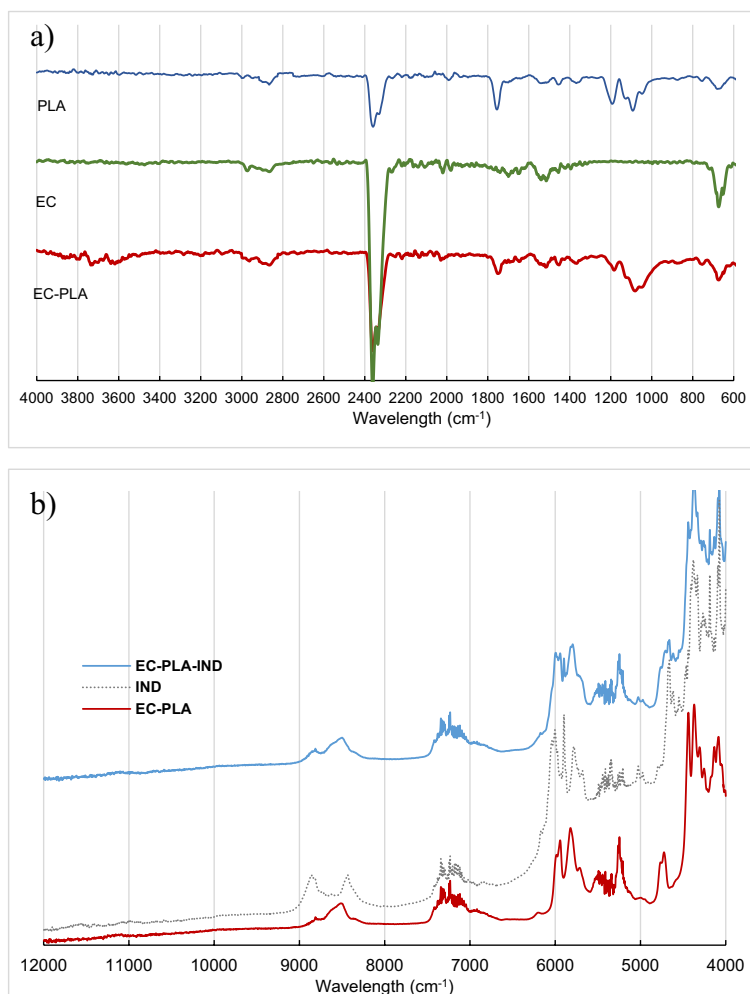

the EC-PLA composite. The second peak, observed at 380 °C for PLA, is at 370 °C for EC and EC-PLA composite.

The TGA analysis shows the degradation of the reference materials and the EC-PLA scaffold (Fig. 3b). All curves showed a one-step weight loss of around 380 °C. This shows that the weight loss of EC-PLA scaffold corresponds to their primary thermal degradation temperatures. However, while the PLA aerogel decomposes completely, there are still some residuals of the EC aerogel after 400 °C. Similar was observed for the EC-PLA scaffold, which also showed some residuals at the same temperature range.

The final structural analysis included testing of the mechanical properties. Achieving mechanical properties that closely resemble those of human bones is crucial for ensuring the longevity and

effectiveness of implants. The analysis included the determination of the compressive moduli, failure stress, and strain of the composite EC-PLA and pure PLA scaffolds. The representative stress–strain curves are presented in Fig. 4a. The compressive strength reached 22.4 MPa for EC-PLA and 26.4 MPa for the pure PLA sample, which is much higher than in the case of the previously reported composite EC-PLA-hydroxyapatite material (HA) (1.57 MPa), prepared by compression moulding (Fig. 4c, EC-PLA-HA) (Mao et al. 2018). Human trabecular bone has a compressive strength of 0.1–30.0 MPa (Keaveny 1998; Birnbaum et al. 2002; Oftadeh et al. 2015), and the developed materials nicely fit this interval. Figure 4b shows the steeper stress–strain curve for the EC-PLA scaffold, which indicates the stiffer material.

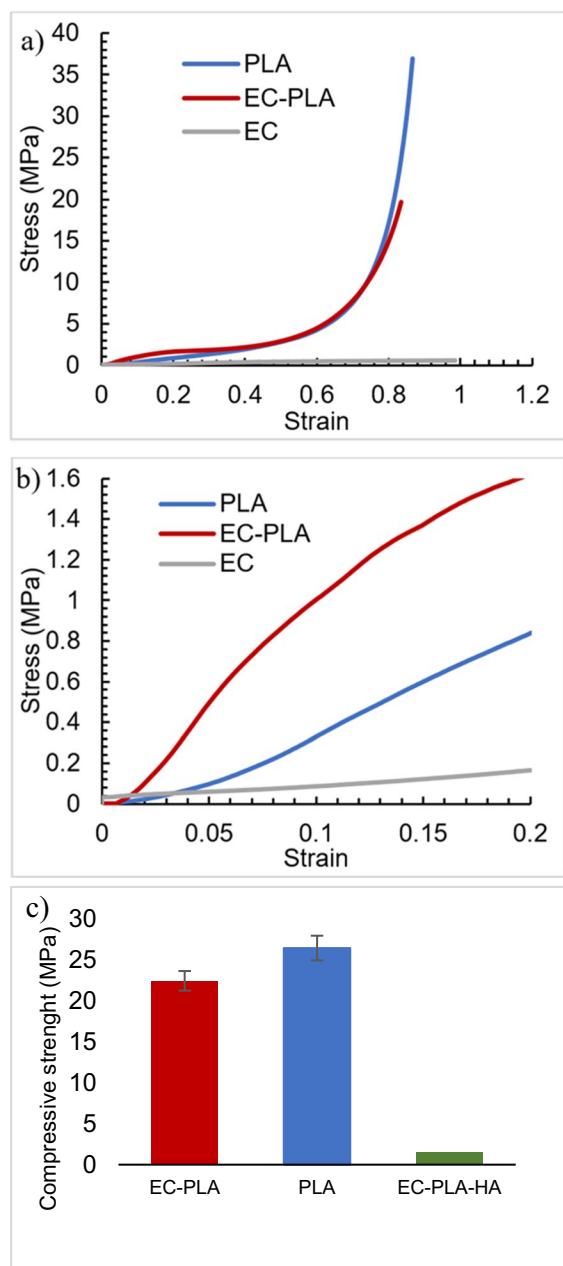**Fig. 3** **a** DSC thermogram, **b** TGA analysis and **c**) DTG analysis
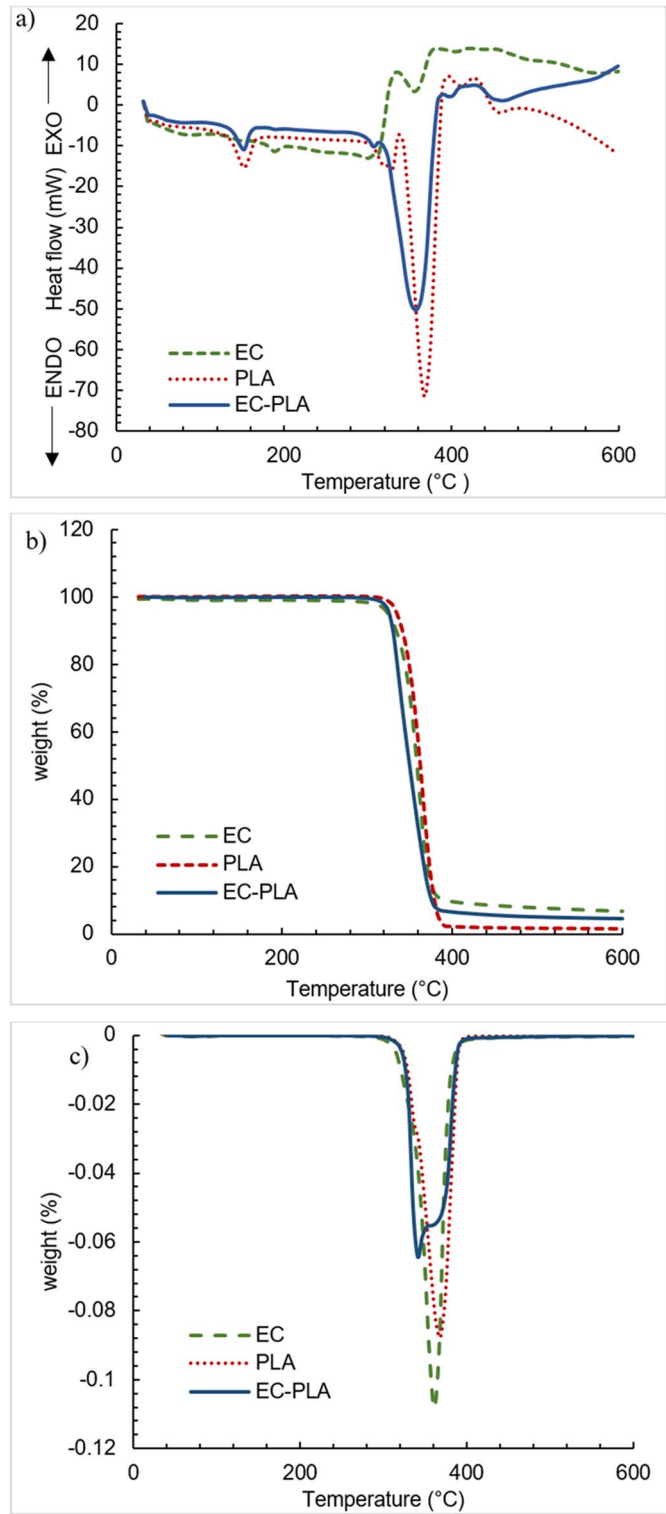
Fig. 4 a Compressive stress–strain curves for PLA, and EC-PLA **b**) close-up of the compressive stress–strain curves up to 0.2% strain, and **c**) compressive strength (error bars represent standard deviations)

The 3D distribution of the indomethacin inside the aerogel

Figure 5 shows 3D ToF–SIMS images of EC-PLA-IND that were sputtered with GCIB (for 10,800 s).

GCIB was used as a sputter gun not to change the chemical composition of the sample during sputtering. Figure 5a and b show the distribution of the $C_{19}H_{15}ClNO_4^-$ and $C_{19}H_{16}ClNO_4^-$ signals at m/z 356.04 and 357.06, respectively, corresponding to the parent ion of indomethacin with the loss of one hydrogen, i.e. $(M–H)^-$ and to the parent ion of indomethacin, i.e. M^-. In positive polarity, a signal for a parent ion ($C_{19}H_{16}ClNO_4^+$; M^+) and the parent ion with the addition of one proton ($C_{19}H_{17}ClNO_4^+$; $(M+H)^+$) were detected (Fig. 5c, d). All these signals were distributed throughout the entire analysed area with locally more intense signals, which is expectable for the formation of aerogel where active ingredients enter the pores of such materials. On the other hand, Fig. 5e shows the distribution of the CH_3^+ signal at m/z 15.02, which mainly originates from the aerogel matrix (EC and PLA).

Drug content, degradation study, and *In vitro* drug dissolution

The degradation of the EC-PLA scaffold was evaluated over 213 days in SBF to determine the possible degradation mechanism of this material in the human body. The experiment was repeated three times, and the mean values with standard deviation are shown in Fig. 6a. The prepared EC-PLA scaffolds started to swell after contact with the SBF, and the weight of the materials increased significantly during the first 4 months of testing. The weight of all three materials doubled after 121 days, which can be attributed to the SBF uptake. The swelling caused the loosening of the pore walls and softening of the material. The addition of PLA to EC improved the materials' properties and preserved this material from degradation. PLA degrades in the body slowly within a year, a reasonable time frame for new bone formation (Ansari 2019). After conducting a comprehensive degradation study over 150 days, we observed the first signs of degradation, evidenced by a gradual decline in the swelling curve. This degradation trend continued up to 213 days, and we expect the material to continue degrading steadily. Those results indicate that the stability of this material exceeds that reported in a previously published study on the combination of EC-PLA-hydroxyapatite composites (Mao et al. 2018), where the 10% of the scaffold was already
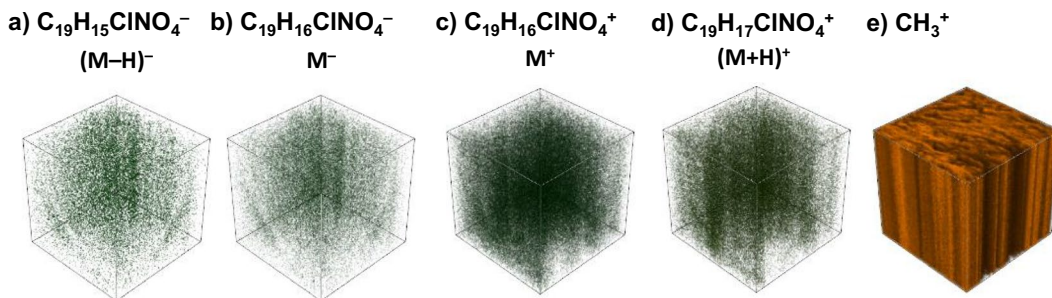
a) $C_{19}H_{15}ClNO_4^-$ (M–H)⁻   b) $C_{19}H_{16}ClNO_4^-$ M⁻   c) $C_{19}H_{16}ClNO_4^+$ M⁺   d) $C_{19}H_{17}ClNO_4^+$ (M+H)⁺   e) CH_3^+

Fig. 5 3D ToF–SIMS imaging of EC-PLA-IND containing indomethacin in **a**, **b**) negative polarity, and **c-e**) in positive polarity
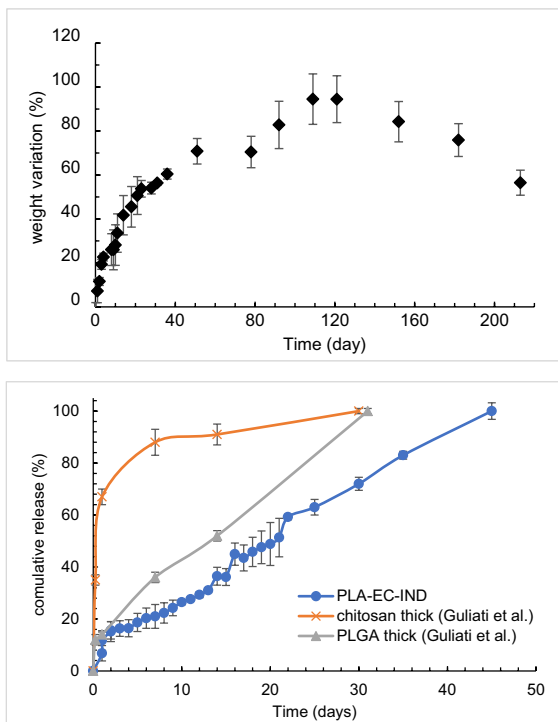
Fig. 6 a Swelling and stability study of the EC-PLA scaffold. **b** IND release from the EC-PLA-IND scaffolds over 7 weeks. The error bars represent standard deviations

degraded after 56 days. The slower degradation rate of our material has the advantage of providing a longer time frame for cell proliferation and growth, which is critical for successful tissue engineering applications.

As mentioned above, IND is soluble in ethanol and was therefore added to the EC solution in the initial step of scaffold preparation. However, due to its solubility in ethanol, drying with supercritical CO_2 may affect the extent of the retained IND in the material. A part of the drug may leave the scaffold during the ethanol extraction process with supercritical CO_2 during supercritical drying. To enable meaningful *in-vitro* drug release testing (as well as to evaluate the therapeutic potential of the incorporated IND), we determined the drug content in the final material after the supercritical drying. Three individual EC-PLA-IND samples were used, and the mean value was calculated with standard deviation. The final drug content in the EC-PLA-IND sample was 18.8 mg ± 1.7 mg of IND/g. The typical oral dose of indomethacin for adults ranges from 25 to 150 mg per day, divided into 2 or 3 doses (Munjal and Allam 2024). However, when drugs are given locally from a bone implant, the amount of drug needed to be given can be much lower as the drug is delivered directly to the area of the body that needs it, reducing the amount that gets metabolized or eliminated in the systemic circulation.

Local delivery of drugs is gaining high interest and is highly desirable in the medical field, especially in tissue engineering. Over the years, immense progress has been achieved in developing tailorable drug release systems for orthopaedic implants (Gulati et al. 2012; Ruan et al. 2022). Herein, IND was loaded onto PLA-EC scaffolds as a representation of water-insoluble drug, in order to demonstrate the drug delivery concept. It has to be pointed out that this approach is not limited to specific drugs and can be applied to a wide range of substances. The dissolution studies herein showed a prolonged IND release from the prepared scaffolds in the phosphate buffer solution for 40 days, and the results are compared with IND release from chitosan and PLGA samples,

reported by Guliati et al. (Gulati et al. 2012). The latter shows the potential of the prepared scaffolds not only to replace damaged trabecular bone but also to therapeutically aid the regeneration process (and/or limit the extent of inflammation that might occur due to implantation). The initial burst dissolution is probably the result of IND residuals on the surface of the scaffold (that occurs either due to the preparation or drying step). Similar effect was reported previously (Gulati et al. 2012). After this burst release for about 2 days, the release slowed and became linear up to 6 weeks, when it reached ~100% of IND release (of the dosage calculated above). The dissolution was performed on three individual samples at the same time points. The results are shown as a graph of average values with standard deviation in Fig. 6b.

Biocompatibility analysis

A series of cell-based tests were performed using primary human osteoblasts to demonstrate the safety and efficacy of the newly developed biodegradable EC-PLA scaffolds with or without incorporated IND. The performed analyses were the live/dead assay (simultaneous staining of live and dead cells), evaluation of morphology (staining of structural actin filaments), cell growth (evaluation of metabolic activity), and phenotypic characterization (staining of osteogenic marker proteins) in the so-called direct contact assay, to show how the cells adhere and grow on the surface of the prepared samples.

First, we evaluated the adhesion and survival of the cells after 24 h and 72 h (Fig. 7a and b, respectively). Cells adhered successfully to both scaffold types, with a higher density observed on the IND-containing scaffolds after both time points, as shown by the green fluorescent staining.

Next, we examined cell morphology and adhesion by staining the cytoskeleton (actin) of the cells. The analysis showed that both scaffold types have good adhesion properties, and cells exhibit a typical cuboid-like osteoblast shape (Fig. 7c), which is in agreement with previous findings. Interestingly, we observed cell aggregates in the IND-containing
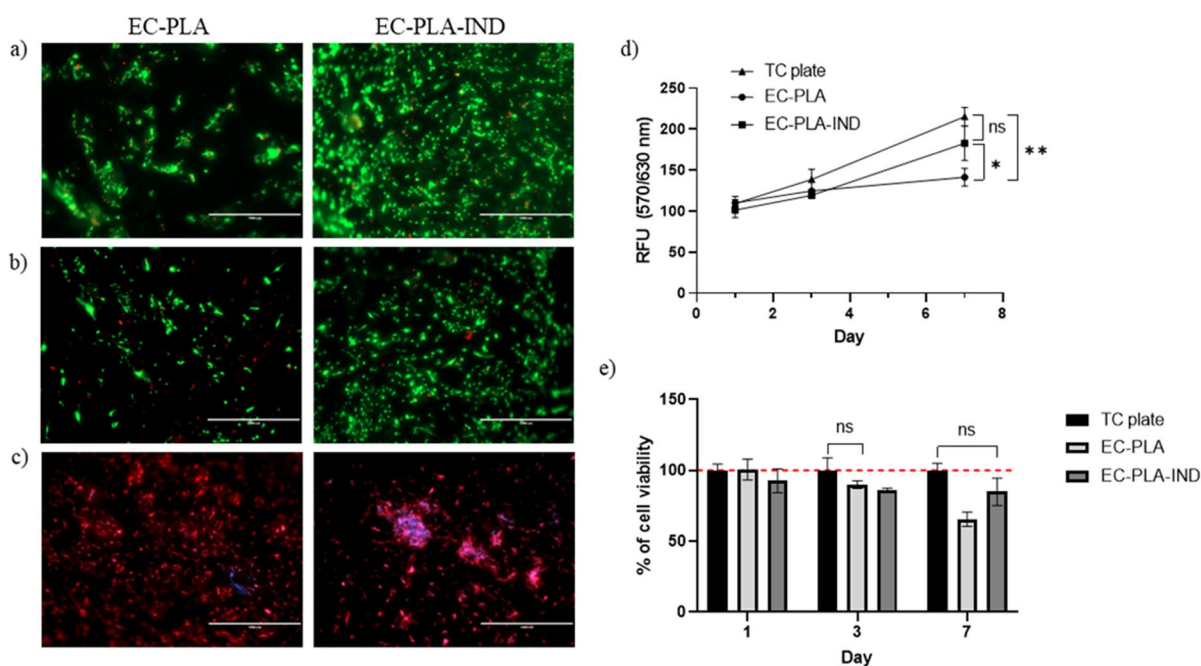

Fig. 7 Cell viability (a, b), morphology (c) and growth (d) of human osteoblast HOB cells in the direct contact assay. (a and b) Fluorescent staining with calcein (green) and P.I. (red). c Fluorescent staining with phalloidin (red) and DAPI (blue). The scale bar indicates 1000 μm. d Metabolic activity assessment with the Alamar Blue (resazurin) assay and comparative cell viability analysis (e). The differences between EC-PLA, EC-PLA-IND and TC plates (* $p < 0.05$; ** $p < 0.005$) were calculated using ANOVA

scaffold that are normally typical of osteoblast cell differentiation. To quantify cell growth and viability (through evaluation of metabolic activity), the Alamar Blue assay was used to analyze the time-dependent changes in total metabolic activity. As shown in Fig. 7d, we observed a significant increase in the metabolic activity of the cells between days, indicating continuous cell growth over 7 days. When comparing the two types of scaffolds (EC-PLA and EC-PLA-IND), we observed a significantly higher cell growth rate on day 7 in scaffolds containing IND ($p = 0.033$). Comparing the two scaffold types and cells grown on tissue culture (TC) plates revealed a significantly slower cell growth for the EC-PLA scaffold but not for the EC-PLA + IND scaffold (Fig. 7d). We further assessed cell viability in relation to TC controls (Fig. 7e), which showed viability exceeding

70% at all time points, indicating satisfactory biocompatibility as per the ISO10993-5 standard.

However, it is important to note that using cells grown on tissue culture plastic as the positive control may not be entirely appropriate due to the distinct topographical features of the tissue engineering scaffolds (such as 3D topology, porosity, and cell ingrowth), which they cannot replicate. On the other hand, flat plates have their distinct specifics, including (often) rapid growth until confluence is reached, followed by contact growth inhibition, which differs from the natural cell growth processes in bone tissue that are influenced by the structure and geometry of the bone (Czekanska et al. 2014; Florencio-Silva et al. 2015). Further investigations are required to explore the behaviour of cells at longer time points, which falls beyond the scope of this manuscript. This

Fig. 8 Immunocytochemical analysis of the osteogenic protein markers collagen type I and osteocalcin (red). The cells were incubated for 10 days prior to immunostaining. The cell nuclei were stained with DAPI (blue). The scale bar indicates 400 μm
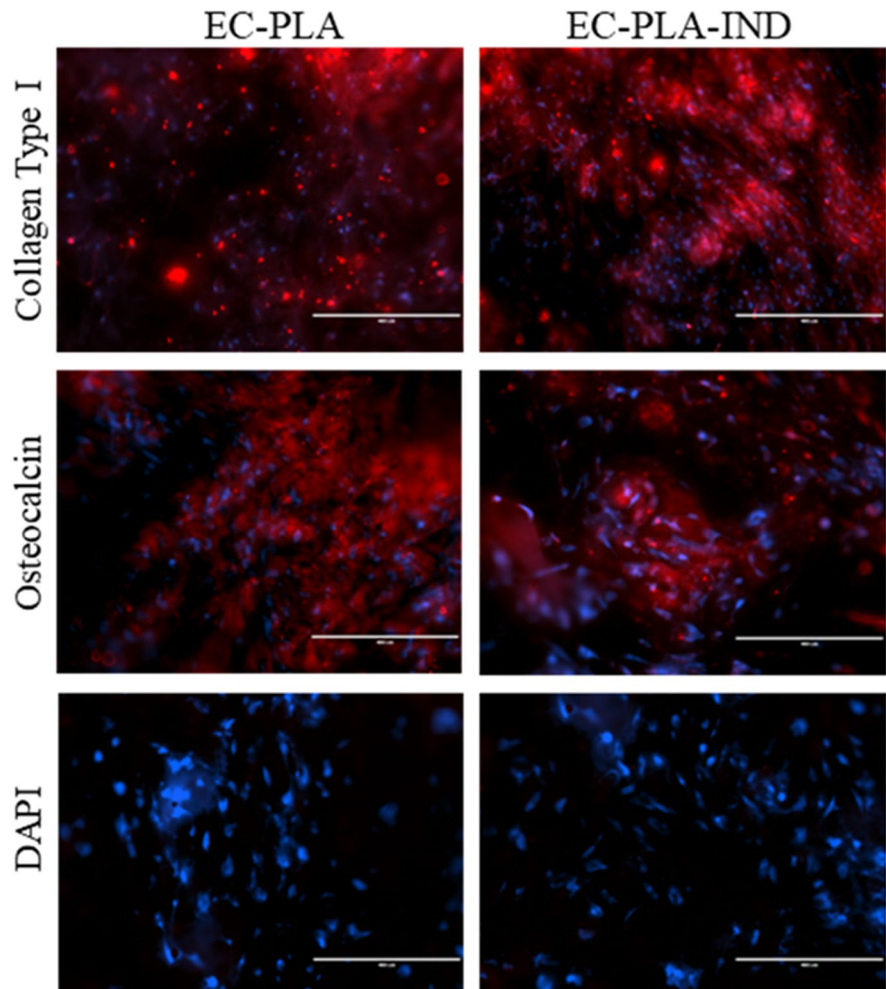
would provide a more comprehensive understanding of the long-term viability and functionality of the scaffolds in supporting cell growth.

Finally, immunocytochemical analysis of the osteogenic protein markers investigated the potential regarding the desired phenotype preservation of the developed biomaterials. As shown in Fig. 8, the expression of collagen type I and osteocalcin was investigated according to the study by Wan et.al (Wan et al. 2022). These results indicate that the HOB cells in direct contact with EC-PLA and EC-PLA-IND scaffolds exhibit a typical osteogenic phenotype (Chuan et al. 2020), with no detectable differences between the scaffolds.

Conclusion

This study presents a novel and innovative approach for combining polylactic acid (PLA) with ethyl cellulose (EC) and using supercritical processes to develop crosslinker-free macro-mesoporous scaffolds. No chemical reaction occurred during the material preparation, and the final material contained interconnected PLA and EC. This structure allows the incorporation of a model drug indomethacin with entrapment efficiency of 17.0% after the supercritical drying. In addition, the mechanical stability of the fabricated materials, with a compressive modulus comparable to that of trabecular bone (22.4 MPa), confirms their potential for bone tissue applications. The drug dissolution of this Biopharmaceutics Classification System BCS III class drug was burst in the first two days, followed by a slower drug release for up to 7 weeks. No degradation of the EC-PLA scaffold was observed in 120 days of immersion in SBF; however, the scaffold could swell and take up to 100% of the SBF compared to its weight. TOF–SIMS analysis showed even distribution of indomethacin throughout the analysed area. Cells adhered successfully to both scaffold types, and we observed a significant increase in the metabolic activity of the cells in consecutive days in both the EC-PLA and EC-PLA-IND scaffolds. Both materials also exhibit a typical osteogenic phenotype, which shows promising results for further *in vivo* studies of those materials. This system offers a significant benefit as it can be utilized with various materials and drugs. Thus, the developed system suits well for a diverse range of orthopedic applications and bone

therapies, including the treatment of bone diseases, local administration of anabolic agents to aid bone repair, antiresorptive agents or targeted treatment in some other specific conditions.

Author's contribution G.H.: Conceptualization, methodology, data curation, formal analysis, writing original draft, funding acquisition, project administration, review and editing. J.R.: Methodology, investigation, writing original draft. U.M.: Conceptualization, validation, supervision, review and editing. M.F.: methodology, investigation, writing original draft, review and editing. Ž.K.: funding acquisition, project administration, review and editing. Z.N.: funding acquisition, conceptualization, project administration, review and editing.

Data availability Not applicable.

Declarations

Ethical approval Not applicable.

Competing interests The authors declare no competing interests.

References

Abbasi N, Hamlet S, Love RM, Nguyen N-T (2020) Porous scaffolds for bone regeneration. J Sci-Adv Mater Dev 5:1–9. https://doi.org/10.1016/j.jsamd.2020.01.007

Ansari M (2019) Bone tissue regeneration: biology, strategies and interface studies. Prog Biomater 8:223–237. https://doi.org/10.1007/s40204-019-00125-z

Birnbaum K, Sindelar R, Gärtner JR, Wirtz DC (2002) Material properties of trabecular bone structures. Surg Radiol Anat 23:399–407. https://doi.org/10.1007/s00276-001-0399-x

Chen P, Bai D, Tang H et al (2022) Polylactide aerogel with excellent comprehensive performances imparted by stereocomplex crystallization for efficient oil-water separation. Polym 255:125128. https://doi.org/10.1016/j.polymer.2022.125128

Chow JW, Chambers TJ (1994) Indomethacin has distinct early and late actions on bone formation induced by mechanical stimulation. Am J Physiol Endocrinol Metab 267:E287–E292. https://doi.org/10.1152/ajpendo.1994.267.2.E287

Choy YB, Choi H, Kim K (2009) Uniform ethyl cellulose microspheres of controlled sizes and polymer viscosities and their drug-release profiles. J Appl Polym Sci 112:850–857. https://doi.org/10.1002/app.29473

Chuan D, Fan R, Wang Y et al (2020) Stereocomplex poly(lactic acid)-based composite nanofiber membranes with highly dispersed hydroxyapatite for potential bone tissue engineering. Compos Sci Technol 192:108107. https://doi.org/10.1016/j.compscitech.2020.108107

Coquard R, Baillis D (2017) Thermal conductivity of Kelvin cell cellulosic aerogels: analytical and Monte Carlo approaches. J Mater Sci 52:11135–11145. https://doi.org/10.1007/s10853-017-0982-0

Cuiffo MA, Snyder J, Elliott AM et al (2017) Impact of the Fused Deposition (FDM) Printing Process on Polylactic Acid (PLA) Chemistry and Structure. Appl Sci 7:579. https://doi.org/10.3390/app7060579

Czekanska EM, Stoddart MJ, Ralphs JR et al (2014) A phenotypic comparison of osteoblast cell lines versus human primary osteoblasts for biomaterials testing. J Biomed Mater Res A 102:2636–2643. https://doi.org/10.1002/jbm.a.34937

Davidovich-Pinhas M, Barbut S, Marangoni AG (2015) The gelation of oil using ethyl cellulose. Carbohydr Polym 117:869–878. https://doi.org/10.1016/j.carbpol.2014.10.035

Dervin S, Pillai SC (2017) An Introduction to Sol-Gel Processing for Aerogels. In: Pillai SC, Hehir S (eds) Sol-Gel Materials for Energy, Environment and Electronic Applications. Springer International Publishing, Cham, pp 1–22

Eurostat: Ageing Europe - statistics on population developments, 15.11.2023. https://ec.europa.eu/eurostat/statistics-explained/index.php?title=Ageing_Europe_-_statistics_on_population_developments

FDA (2016) The Biopharmaceutics Classification System (BCS) Guidance

Fernandez de Grado G, Keller L, Idoux-Gillet Y et al (2018) Bone substitutes: a review of their characteristics, clinical use, and perspectives for large bone defects management. J Tissue Eng 9:204173141877681. https://doi.org/10.1177/2041731418776819

Ferreira-Gonçalves T, Constantin C, Neagu M et al (2021) Safety and efficacy assessment of aerogels for biomedical applications. Biomed Pharmacother 144:112356. https://doi.org/10.1016/j.biopha.2021.112356

Finšgar M, Uzunalić AP, Stergar J et al (2016) Novel chitosan/diclofenac coatings on medical grade stainless steel for hip replacement applications. Sci Rep 6:26653. https://doi.org/10.1038/srep26653

Finšgar M, Kovač J, Maver U (2021) The development and characterization of bioactive coatings for local drug delivery in orthopedic applications. Prog Org Coat 158:106350. https://doi.org/10.1016/j.porgcoat.2021.106350

Florencio-Silva R, Sasso GRDS, Sasso-Cerri E et al (2015) Biology of Bone Tissue: Structure, Function, and Factors That Influence Bone Cells. Biomed Res Int 2015:1–17. https://doi.org/10.1155/2015/421746

García-González CA, Smirnova I (2013) Use of supercritical fluid technology for the production of tailor-made aerogel particles for delivery systems. J Supercrit Fluids 79:152–158. https://doi.org/10.1016/j.supflu.2013.03.001

García-González CA, Sosnik A, Kalmár J et al (2021) Aerogels in drug delivery: From design to application. JCR 332:40–63. https://doi.org/10.1016/j.jconrel.2021.02.012

Gulati K, Ramakrishnan S, Aw MS et al (2012) Biocompatible polymer coating of titania nanotube arrays for improved drug elution and osteoblast adhesion. Acta Biomater 8:449–456. https://doi.org/10.1016/j.actbio.2011.09.004

Horvat G, Fajfar T, Uzunalić AP et al (2016) Thermal properties of polysaccharide aerogels. J Therm Anal Calorim 127:363–370. https://doi.org/10.1007/s10973-016-5814-y

Horvat G, Xhanari K, Finšgar M et al (2017) Novel ethanol-induced pectin–xanthan aerogel coatings for orthopedic applications. Carbohydr Polym 166:365–376. https://doi.org/10.1016/j.carbpol.2017.03.008

Horvat G, Pantić M, Knez Ž, Novak Z (2018) Encapsulation and drug release of poorly water soluble nifedipine from bio-carriers. J Non-Cryst Solids 481:486–493. https://doi.org/10.1016/j.jnoncrysol.2017.11.037

Horvat G, Pantić M, Knez Ž, Novak Z (2022) A Brief Evaluation of Pore Structure Determination for Bioaerogels. Gels 8:438. https://doi.org/10.3390/gels8070438

Janmohammadi M, Nazemi Z, Salehi AOM et al (2022) Cellulose-based composite scaffolds for bone tissue engineering and localized drug delivery. Bioact Mater 20:137–163. https://doi.org/10.1016/j.bioactmat.2022.05.018

Junior Maksoud F, de la Paz MFV, Hann AJ et al (2022) Porous biomaterials for tissue engineering: a review. J Mater Chem B 10(40):8111–8165. https://doi.org/10.1039/D1TB02628C

Kapur S, Baylink DJ, William Lau K-H (2003) Fluid flow shear stress stimulates human osteoblast proliferation and differentiation through multiple interacting and competing signal transduction pathways. Bone 32:241–251. https://doi.org/10.1016/S8756-3282(02)00979-1

Keaveny TM (1998) Cancellous bone. In: Black J, Hastings G (eds) Handbook of Biomaterial Properties. Springer, US, Boston, MA, pp 15–23

Kistler SS (1931) Coherent Expanded Aerogels and Jellies. Nature 127:741–741. https://doi.org/10.1038/127741a0

Kloc AP, Danzer A, Sadowski G (2023) Solubility of naproxen and indomethacin in supercritical carbon dioxide/ethyl

acetate mixtures. J Supercrit Fluids 200:105990. https://doi.org/10.1016/j.supflu.2023.105990

Knez Ž, Markočič E, Leitgeb M et al (2014) Industrial applications of supercritical fluids: A review. Energy 77:235–243. https://doi.org/10.1016/j.energy.2014.07.044

Kokubo T, Kushitani H, Sakka S et al (1990) Solutions able to reproducein vivo surface-structure changes in bioactive glass-ceramic A-W3. J Biomed Mater Res 24:721–734. https://doi.org/10.1002/jbm.820240607

Kravanja KA, Finšgar M, Knez Ž, Knez Marevci M (2022) Supercritical Fluid Technologies for the Incorporation of Synthetic and Natural Active Compounds into Materials for Drug Formulation and Delivery. Pharmaceutics 14:1670. https://doi.org/10.3390/pharmaceutics14081670

Liu T, Huang K, Li L et al (2019) High performance high-density polyethylene/hydroxyapatite nanocomposites for load-bearing bone substitute: fabrication, in vitro and in vivo biocompatibility evaluation. Compos Sci Technol 175:100–110. https://doi.org/10.1016/j.compscitech.2019.03.012

Lutzweiler G, Ndreu Halili A, Engin Vrana N (2020) The Overview of Porous, Bioactive Scaffolds as Instructive Biomaterials for Tissue Regeneration and Their Clinical Translation. Pharmaceutics 12:602. https://doi.org/10.3390/pharmaceutics12070602

Mao D, Li Q, Bai N et al (2018) Porous stable poly(lactic acid)/ethyl cellulose/hydroxyapatite composite scaffolds prepared by a combined method for bone regeneration. Carbohydr Polym 180:104–111. https://doi.org/10.1016/j.carbpol.2017.10.031

Mastnak T, Maver U, Finšgar M (2022) Addressing the Needs of the Rapidly Aging Society through the Development of Multifunctional Bioactive Coatings for Orthopedic Applications. Int J Mol Sci 23:2786. https://doi.org/10.3390/ijms23052786

Maver U, Xhanari K, Žižek M et al (2018) A combination of interdisciplinary analytical tools for evaluation of multi-layered coatings on medical grade stainless steel for biomedical applications. Eur J Pharm Biopharm 128:230–246. https://doi.org/10.1016/j.ejpb.2018.05.002

Mccarthy TL, Centrella M, Raisz LG, Canalis E (1991) Prostaglandin E2 Stimulates Insulin-Like Growth Factor I Synthesis in Osteoblast-Enriched Cultures from Fetal Rat Bone*. Endocrinology 128:2895–2900. https://doi.org/10.1210/endo-128-6-2895

Melo P, Ferreira A-M, Waldron K et al (2019) Osteoinduction of 3D printed particulate and short-fibre reinforced composites produced using PLLA and apatite-wollastonite. Compos Sci Technol 184:107834. https://doi.org/10.1016/j.compscitech.2019.107834

Muhammad A, Lee D, Shin Y, Park J (2021) Recent Progress in Polysaccharide Aerogels: Their Synthesis, Application, and Future Outlook. Polymers (basel) 13:1347. https://doi.org/10.3390/polym13081347

Munjal A, Allam AE (2024) Indomethacin. In: StatPearls. Treasure Island (FL): StatPearls Publishing. http://www.ncbi.nlm.nih.gov/books/NBK555936/

Nie B, Huo S, Qu X et al (2022) Bone infection site targeting nanoparticle-antibiotics delivery vehicle to enhance treatment efficacy of orthopedic implant related infection. Bioact Mater 16:134–148. https://doi.org/10.1016/j.bioactmat.2022.02.003

Novak Z, Knez Ž (1997) Diffusion of methanol–liquid CO2 and methanol–supercritical CO2 in silica aerogels. J Non-Cryst Solids 221:163–169

Oftadeh R, Perez-Viloria M, Villa-Camacho JC et al (2015) Biomechanics and Mechanobiology of Trabecular Bone: A Review. J Biomech Eng 137:010802. https://doi.org/10.1115/1.4029176

Oladapo BI, Obisesan OB, Oluwole B et al (2020) Mechanical characterization of a polymeric scaffold for bone implant. J Mater Sci 55:9057–9069. https://doi.org/10.1007/s10853-020-04638-y

Peeters A, Putzeys G, Thorrez L (2019) Current Insights in the Application of Bone Grafts for Local Antibiotic Delivery in Bone Reconstruction Surgery. J Bone Joint Infect 4:245–253. https://doi.org/10.7150/jbji.38373

Pircher N, Carbajal L, Schimper C et al (2016) Impact of selected solvent systems on the pore and solid structure of cellulose aerogels. Cellul 23:1949–1966. https://doi.org/10.1007/s10570-016-0896-z

Pradhan S, Brooks AK, Yadavalli VK (2020) Nature-derived materials for the fabrication of functional biodevices. Mater Today Bio 7:100065. https://doi.org/10.1016/j.mtbio.2020.100065

Rege A, Schestakow M, Karadagli I et al (2016) Micromechanical modelling of cellulose aerogels from molten salt hydrates. Soft Matter 12:7079–7088. https://doi.org/10.1039/C6SM01460G

Rege A, Preibisch I, Schestakow M et al (2018) Correlating Synthesis Parameters to Morphological Entities: Predictive Modeling of Biopolymer Aerogels. Mater 11:1670. https://doi.org/10.3390/ma11091670

Ribas RG, Schatkoski VM, Montanheiro TLDA et al (2019) Current advances in bone tissue engineering concerning ceramic and bioglass scaffolds: A review. Ceram Int 45:21051–21061. https://doi.org/10.1016/j.ceramint.2019.07.096

Ruan L, Su M, Qin X et al (2022) Progress in the application of sustained-release drug microspheres in tissue engineering. Mater Today Bio 16:100394. https://doi.org/10.1016/j.mtbio.2022.100394

Tian B, Tang S, Li Y et al (2014) Fabrication, characterization, and biocompatibility of ethyl cellulose/carbonated hydroxyapatite composite coatings on Ti6Al4V. J Mater Sci: Mater Med 25:2059–2068. https://doi.org/10.1007/s10856-014-5239-8

Tkalec G, Knez Ž, Novak Z (2015) Formation of polysaccharide aerogels in ethanol. RSC Adv 5:77362–77371. https://doi.org/10.1039/C5RA14140K

Tran TB, Tran TH, Vu YH et al (2021) pH-responsive nanocarriers for combined chemotherapies: a new approach with old materials. Cellul 28:3423–3433. https://doi.org/10.1007/s10570-021-03769-y

Veronovski A, Tkalec G, Knez Ž, Novak Z (2014) Characterisation of biodegradable pectin aerogels and their potential use as drug carriers. Carbohydr Polym 113:272–278. https://doi.org/10.1016/j.carbpol.2014.06.054

Wan H-Y, Shin RLY, Chen JCH et al (2022) Dextran sulfate-amplified extracellular matrix deposition promotes osteogenic differentiation of mesenchymal stem cells. Acta Biomater 140:163–177. https://doi.org/10.1016/j.actbio.2021.11.049

Wang Y, Gao M, Pan X et al (2023) Preparation of resveratrol-loaded ethyl cellulose microspheres via foam-transfer and its application performances. Cellul 30:6401–6421. https://doi.org/10.1007/s10570-023-05274-w

Wasilewska K, Winnicka K (2019) Ethylcellulose-A Pharmaceutical Excipient with Multidirectional Application in Drug Dosage Forms Development. Materials (basel) 12:E3386. https://doi.org/10.3390/ma12203386

Weiser JR, Saltzman WM (2014) Controlled Release for Local Delivery of Drugs: Barriers and Models. J Control Release 190:664–673. https://doi.org/10.1016/j.jconrel.2014.04.048

WHO (2022) Ageing and health. https://www.who.int/news-room/fact-sheets/detail/ageing-and-health

Wu Z, Chan B, Low J et al (2022) Microbial resistance to nanotechnologies: An important but understudied consideration using antimicrobial nanotechnologies in orthopaedic implants. Bioact Mater. https://doi.org/10.1016/j.bioactmat.2022.02.014

Zan J, Qian G, Deng F et al (2022) Dilemma and breakthrough of biodegradable poly-l-lactic acid in bone tissue repair. J Mater Res Technol 17:2369–2387. https://doi.org/10.1016/j.jmrt.2022.01.164